Phytopathology Research

RESEARCH

Open Access

# An increase in the number of peroxisomes is coupled to the initial infection stage and stress response of *Botrytis cinerea*

Hongjia Han, Xuejing Niu, Wenxing Liang* and Mengjie Liu*

## Abstract

Peroxisomes are very important organelles in eukaryotic cells and participate in various biological processes, including pathogen–host interactions. A variety of proteins involved in peroxisome proliferation and metabolic activity within peroxisomes have been shown to be essential for full virulence of several phytopathogenic fungi. However, the effects of changes in the number of peroxisomes and proteins involved in the peroxisome pathway on the pathogenicity of *Botrytis cinerea* have rarely been reported. In this study, by analysing transcriptome data and RT-qPCR validation, we found that more than half of the genes annotated to the peroxisome pathway in *B. cinerea* were upregulated more than twofold between mycelial samples cultured in medium with tomato leaves and without tomato leaves. A strain of *B. cinerea* with fluorescently labelled peroxisomes was obtained by overexpression of GFP fused to peroxisomal targeting signal 1 (the tripeptide 'SKL'). The addition of tomato leaves to the liquid medium induced a significant increase in the number of peroxisomes, β-oxidation level, $H_2O_2$ content, and acetyl-CoA level in *B. cinerea* mycelia. When *B. cinerea* was cultured with oleic acid as the sole carbon source, the formation of infection-related structures and their penetration into plant cells were found to be associated with peroxisome pathway activity. Furthermore, peroxisome proliferation and lipid metabolism increased in response to different extracellular stresses in *B. cinerea*. Taken together, our results confirmed that activation of the peroxisome pathway in *B. cinerea* contributes to the initial infection and the ability to cope with environmental stress.

**Keywords:** *Botrytis cinerea*, Peroxisome, Lipid metabolism, Infection, Environmental stress

## Background

*Botrytis cinerea*, the causal agent of grey mould disease, is one of the most invasive pathogens and affects more than 1000 species of 586 plant genera, including numerous agriculturally important crop cultivars (Dean et al. 2012; Elad et al. 2016a). As a typical necrotrophic plant pathogen, *B. cinerea* can attack different plant tissues, causing enormous pre- and post-harvest crop loss and leading to incalculable economic loss annually (Elad et al. 2016b; Soltis et al. 2019). During pathogenesis, *B. cinerea* releases a large number of virulence factors, most of which are proteins that regulate the production or catabolism of reactive oxygen species (ROS), various proteases (cutinases, lipases, glycosyl hydrolases, pectin methylesterases, etc.) that degrade components of the host cuticle and cell wall or generate assimilable nutrients, or various pathogen-associated molecular patterns that suppress the host immune system (González et al. 2016; Siegmund and Viefhues 2016). Currently, chemical control based on the application of chemical fungicides remains the easiest and most effective way to manage grey mould epidemics in many crop species (Fillinger and Walker 2016). However, under long-term selective pressure, *B. cinerea* has developed varying degrees of

*Correspondence: wliang1@qau.edu.cn; mjliu@qau.edu.cn

College of Plant Health and Medicine, Qingdao Agricultural University, Qingdao 266109, China

tolerance to almost all fungicides, which severely weakens the control efficacy of these fungicides on grey mould (Hu et al. 2016). Point mutations in drug targets of *B. cinerea* are mainly responsible for high levels of resistance to fungicides with site-specific activity (Chatzidimopoulos et al. 2016). Therefore, new targets need to be identified to explore more effective fungicides to control the occurrence of *B. cinerea*.

Peroxisomes are a class of ubiquitous and crucial organelles that perform a variety of important cellular functions in nearly all eukaryotic cells (Wanders 2013; Islinger et al. 2018). In accomplishing cellular tasks or in response to various environmental stimuli, the abundance of peroxisomes can be changed and coordinated through several cellular processes, including peroxisome biogenesis, proliferation, and degradation (Smith and Aitchison 2013; Chen et al. 2016). The assembly of peroxisome biogenesis proteins (collectively called peroxins) is required for the biogenesis and proliferation of peroxisomes and the import of proteins into the peroxisomal matrix (Distel et al. 1996; Smith and Aitchison 2013). To date, more than 30 peroxins have been shown to function in peroxisome formation; among them, 3 peroxins have been characterized as import receptors that recognize peroxisomal matrix proteins, including peroxisomal targeting signal 1 or 2 (PTS1 or PTS2) (Stanley et al. 2007; Kong et al. 2019). The conserved functions of peroxisomes include β-oxidation of fatty acids and metabolism of hydrogen peroxide ($H_2O_2$). In filamentous fungi, peroxisomes are also involved in many other metabolic pathways, such as the biogenesis of Woronin bodies (WBs) and secondary metabolites, all of which are important for fungal development and pathogenesis (van der Klei and Veenhuis 2013; Chen et al. 2016). β-Oxidation of fatty acids in peroxisomes can lead to an abundance of acetyl-coenzyme A (acetyl-CoA), which can be used for the biosynthesis of polyketides and biotin, the production of glucose via the glyoxylate cycle and gluconeogenesis, and the synthesis of melanin and cell wall components (van der Klei and Veenhuis 2013; Chen et al. 2016).

The functions of peroxisomes have been studied in various organisms, and increasing amounts of evidence have shown that peroxisomes and several peroxins are essential for the pathogenicity of several plant pathogenic fungi (Kubo 2013; Chen et al. 2016). In the anthracnose-causing fungus *Colletotrichum orbiculare*, appressorial melanization and penetration depend on β-oxidation and the peroxins PEX6, PEX13, and MEF (Kimura et al. 2001; Fujihara et al. 2010; Asakura et al. 2012). In *Fusarium graminearum*, the peroxins PEX5, PEX6, PEX13, PEX14, PEX33, PEX4, and PEX2 have been reported to be associated with pathogenicity (Min et al. 2012; Chen et al. 2018; Zhang et al. 2019; Wang et al. 2020). An overview of the relationship between peroxisomes and pathogenicity in the rice blast fungus *Magnaporthe oryzae* has also been provided (Chen et al. 2016). Multiple proteins that play important roles in the maintenance of peroxisomal functions in *M. oryzae* have been reported to be associated with pathogenicity. Specifically, single-deletion mutants of several of these proteins, such as PEX19, PEX5, PEX6, and PEX7, exhibited complete loss of pathogenicity (Chen et al. 2016). The role of peroxisomal proteins in pathogenesis of various plant pathogens has gradually become clear. However, most relevant studies have focused on the phenotypic changes resulting from the deletion of a certain peroxisomal protein, and little attention has been given to the relationship between the number of peroxisomes and pathogenicity. Moreover, the roles of peroxisomes in *B. cinerea* have not been studied extensively.

In this study, we focused on the overall changes in peroxisomes in *B. cinerea*. Using reverse transcription-quantitative PCR (RT-qPCR), we measured the expression levels of genes annotated to the peroxisome pathway and labelled peroxisomes with green fluorescent protein (GFP) to observe quantitative changes. Our results demonstrate that the number of intracellular peroxisomes and β-oxidation in *B. cinerea* is significantly increased during the initial infection stage and in response to different culture conditions and environmental stimuli.

## Results

### Genes annotated to the peroxisome pathway in *B. cinerea* were differentially expressed at the initial stage of infection

To investigate the involvement of the peroxisome pathway in the early stages of *B. cinerea* infection, we analysed transcriptomic data to identify the corresponding genes. A total of 66 genes were annotated to the peroxisome pathway (Kyoto Encyclopedia of Genes and Genomes (KEGG) pathway bfu04146), of which 38 were differentially expressed by more than twofold ($P$ value < 0.05) between *B. cinerea* cultured in medium with tomato leaves (BcT) and without tomato leaves (BcU) according to the transcriptomic data of three biological replicates (Fig. 1 and Additional file 1: Table S1). Among these 38 genes, 34 and 4 genes were upregulated and downregulated, respectively, at 6 h after induction with tomato leaves versus without tomato leaves (BcU vs. BcT). These differentially expressed genes (DEGs) were mainly involved in the process of peroxisome formation (biogenesis, elongation, and fission), fatty acid β-oxidation, and ROS homeostasis in the peroxisome pathway (Fig. 1).

The relative expression levels of 12 representative DEGs (10 upregulated and 2 downregulated) were validated by RT-qPCR. Hierarchical cluster analysis was

performed based on the relative expression levels of these 12 genes in 9 samples (conidia at 0 h and germinated conidia collected at 3, 6, 9, and 12 h post-inoculation (hpi) from medium with or without tomato leaves). The results showed that the samples induced by the addition of tomato leaves clustered together, while the samples without leaf induction clustered together (Fig. 2a). The expression levels of the 12 genes were significantly upregulated at the germination stage (3, 6, 9, and 12 hpi) compared with those at the conidial stage (0 h) (Fig. 2b). Importantly, the expression levels of the 10 upregulated DEGs in the samples with leaf induction were significantly higher than those in the samples without leaf induction at the germination stage (Fig. 2b). In addition, the expression levels of 2 downregulated DEGs in the samples with leaf induction were lower than those in the samples without leaf induction at 3, 6, and 9 hpi, and the levels with and without leaf induction were the same at 12 hpi (Fig. 2b).

### Bioinformatics analysis of *B. cinerea* genes annotated to the peroxisome pathway

To further understand the functions of these DEGs, Gene ontology (GO) enrichment analysis, BLAST searches of the pathogen–host interaction (PHI) database, and protein–protein interaction (PPI) analysis were performed. Three DEGs were enriched in the biological process category, 5 DEGs were enriched in the cellular component category, and 9 DEGs were enriched in the molecular function category, with a threshold of $P<0.05$ (Additional file 2: Figure S1a and Additional file 1: Table S2). Among the proteins encoded by 37 DEGs, 27 were assigned to the PHI database, with an e-value < 1E-5 cut-off. Of these proteins, 7 belonged to the loss of pathogenicity category, and 16 and 1 were associated with reduced virulence and increased virulence, respectively (Additional file 2: Figure S1b and Additional file 1: Table S3). Twenty-two proteins were mapped to an interaction network with a medium confidence score of 0.4 and were shown to cluster into three groups via the Markov cluster (MCL) algorithm (Additional file 2: Figure S1c).

### Visualization of peroxisomes in *B. cinerea* via SKL-tagged GFP without affecting fungal growth and development

To visualize the peroxisomes, we tagged the C-terminus of GFP with the PTS1 tripeptide SKL, a widely used peroxisomal targeting signal, and then transformed the construct into the protoplasts of *B. cinerea* (Fig. 3a). There was no significant difference in mycelial growth and conidial production between the wild-type strain B05.10 and the transformants GFP-SKL-1 and GFP-SKL-2 (Fig. 3b–d). Under fluorescence microscopy, the fluorescence produced by these two transformants (represented by GFP-SKL-1) was present in a punctate pattern throughout the cytoplasm, while the fluorescence produced by GFP only (GFP with no SKL tag) was distributed evenly throughout the cell (Fig. 3e). These punctate structures did not overlap with the nucleus (stained with 4′,6-diamidino-2-phenylindole (DAPI)) and were smaller than the nucleus (Fig. 3e). Western blot analysis showed that both GFP-SKL and GFP were expressed in the corresponding strains (Fig. 3f).

Lipids have been shown to induce an increase in the number of peroxisomes (Chen et al. 2017). When Tween-80 was used as the sole carbon source, the number of fluorescent punctate structures in conidia and hyphae was increased at 6 and 9 hpi compared with that cultured in yeast extract peptone dextrose (YEPD) liquid medium (Additional file 2: Figure S2a, b). In particular, the number of fluorescent punctate structures per unit of hyphal length (0.1 mm) in strain GFP-SKL grown in Tween-80 was significantly higher than that in YEPD medium (Additional file 2: Figure S2c, d). As expected, the distribution and the increase in the number of fluorescent punctate structures were consistent with the known marker for peroxisomes, indicating that the peroxisomes of *B. cinerea* were indeed marked by GFP and could be observed under fluorescence microscope.

### The peroxisome pathway in *B. cinerea* was activated at the initial stage of infection

Changes in the number of peroxisomes were observed and quantified in the *B. cinerea* strain GFP-SKL cultured in YEPD medium with or without tomato leaves (Fig. 4a, b). The results showed that when tomato leaves were added to the medium, the number of peroxisomes in the hyphae of GFP-SKL was significantly ($P<0.01$) greater than that in the medium without leaves at 6 hpi, but in the conidia, no significant difference ($P>0.05$) in peroxisome numbers was found between these two treatments; at 9 hpi, the number of peroxisomes in both the hyphae and the conidia under the induction with leaves

(See figure on next page.)

**Fig. 1** Cluster analysis of the DEGs annotated to the peroxisome pathway in *B. cinerea* (KEGG pathway: bfu04146). A total of 38 DEGs with a threshold of $|\log2(FC)|\geq 1$ and *P* value < 0.05 were used for heatmap construction based on samples and expression patterns from RNA sequencing data. The coloured squares indicate the range of expression according to fragments per kilobase of exon per million fragments mapped (FPKM) values in different samples (biological replicates). BcU, mycelial samples without tomato leaf induction. BcT, mycelial samples with tomato leaf induction. FC, fold change of BcT/BcU

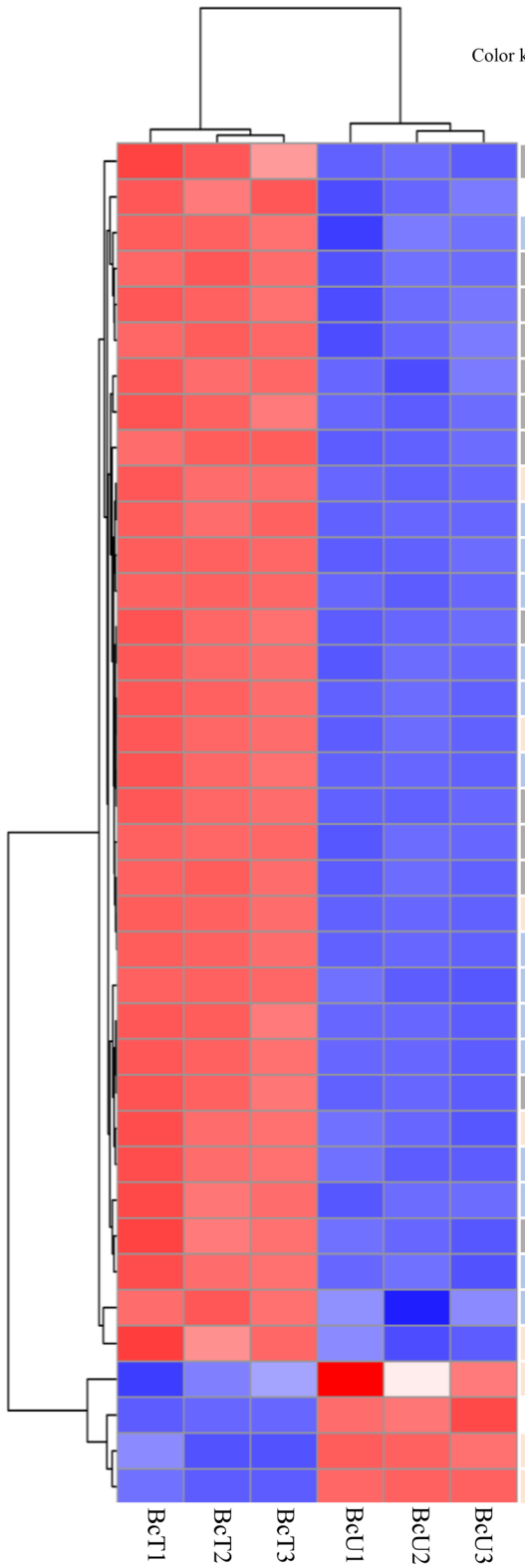


| Gene locus | FC* | Protein name | Stage in Peroxisome Pathway |
|---|---|---|---|
| Bcin08g02900 | 2.13±0.19 | / | Peroxisome formation |
| Bcin13g00810 | 3.35±0.22 | Bcdao3 | Amino acid metabolism |
| Bcin16g02260 | 2.00±0.04 | / | Fatty acid-oxidation |
| Bcin01g10600 | 2.68±0.08 | Bcpex1 | Peroxisome formation |
| Bcin01g02750 | 2.72±0.09 | Bcpex10 | Peroxisome formation |
| Bcin02g03780 | 3.63±0.06 | Bcpex6 | Peroxisome formation |
| Bcin15g01560 | 4.45±0.23 | / | Peroxisome formation |
| Bcin06g07080 | 3.13±0.19 | Bcpex7 | Peroxisome formation |
| Bcin07g03000 | 5.20±0.21 | / | Peroxisome formation |
| Bcin03g03390 | 9.97±0.68 | Bcsod1 | Antioxidant system |
| Bcin04g06330 | 8.37±0.42 | / | Fatty acid-oxidation |
| Bcin14g02030 | 22.91±0.95 | / | Fatty acid-oxidation |
| Bcin09g01530 | 15.29±0.25 | Bctes1 | Fatty acid-oxidation |
| Bcin11g00350 | 3.70±0.18 | Bcpex14 | Peroxisome formation |
| Bcin04g00760 | 4.48±0.19 | Bcfaa2 | Fatty acid-oxidation |
| Bcin12g00940 | 4.21±0.16 | / | Fatty acid-oxidation |
| Bcin10g02820 | 8.15±0.49 | / | Antioxidant system |
| Bcin01g07920 | 4.13±0.23 | Bcsps19 | Fatty acid-oxidation |
| Bcin13g02740 | 7.25±0.47 | Bcpex11 | Peroxisome formation |
| Bcin12g06240 | 3.32±0.03 | Bcpex12 | Peroxisome formation |
| Bcin05g05280 | 3.23±0.07 | Bcpex13 | Peroxisome formation |
| Bcin13g00770 | 7.27±0.33 | / | Antioxidant system |
| Bcin03g07910 | 8.56±0.32 | Bccat2 | Fatty acid-oxidation |
| Bcin14g02960 | 11.23±0.18 | / | Fatty acid-oxidation |
| Bcin04g05130 | 2.12±0.08 | Bcpxa2 | Fatty acid-oxidation |
| Bcin03g03940 | 6.18±0.40 | / | Fatty acid-oxidation |
| Bcin05g06540 | 2.79±0.13 | / | Peroxisome formation |
| Bcin01g03830 | 3.04±0.18 | Bcsod3 | Antioxidant system |
| Bcin04g03710 | 4.33±0.30 | / | Fatty acid-oxidation |
| Bcin01g07620 | 3.75±0.31 | Bcpcd1 | Fatty acid-oxidation |
| Bcin04g04470 | 2.48±0.18 | Bcpex19 | Peroxisome formation |
| Bcin15g02650 | 2.40±0.11 | Bcnpy1 | Fatty acid-oxidation |
| Bcin15g01860 | 2.02±0.05 | / | Fatty acid-oxidation |
| Bcin05g04580 | 3.63±0.43 | Bccat6 | Antioxidant system |
| Bcin09g04400 | 0.18±0.10 | Bccat7 | Antioxidant system |
| Bcin12g02310 | 0.36±0.01 | / | Purine metabolism |
| Bcin10g01030 | 0.49±0.03 | Bcprx9 | Antioxidant system |
| Bcin06g01180 | 0.07±0.01 | BccatA | Antioxidant system |

*, the fold change of BcU vs BcT (BcT/BcU), mean ± SD.

**Fig. 1** (See legend on previous page.)

was slightly higher than that without leaves. However, there was no statistically significant difference ($P>0.1$) in hyphal length between the two groups (Fig. 4c). Malondialdehyde (MDA) is a common lipid peroxidation product and is widely used as a biomarker for lipid peroxidation and ROS accumulation (Miret et al. 2018). When tomato leaves were added to the medium, the MDA content in the mycelia was significantly ($P<0.01$) increased at 9 hpi compared with that in the medium with no leaves (Fig. 4d), indicating that the presence of tomato leaves increased lipid oxidation in *B. cinerea* mycelia. The lipid β-oxidation process is accompanied by the generation of large amounts of ROS, which are scavenged in peroxisomes to maintain ROS homeostasis in cells (Knoblach et al. 2013; Tripathi et al. 2016). However, when tomato leaves were added to the medium, the $H_2O_2$ content in *B. cinerea* mycelia was significantly ($P<0.01$) higher than that in the medium with no tomato leaves at both 6 and 9 hpi (Fig. 4e). In addition, under induction with tomato leaves, the accumulation level of acetyl-CoA in mycelia was significantly higher than that without tomato leaves (Fig. 4f), which may allow *B. cinerea* to synthesize more secondary metabolites to infect the host (van der Klei and Veenhuis 2013; Chen et al. 2016).

### Fatty acids induced an increase in the number of peroxisomes and the formation of infection structures of *B. cinerea*

It has been reported that fructose can promote the formation of appressorium (AP)-like structures in *B. cinerea* (Liu et al. 2018). To understand the potential relationship between the activation of the peroxisome pathway and the infection ability of *B. cinerea* at the early infection stage, the numbers of peroxisomes and AP-like structures were quantified under different culture conditions (Fig. 5). Under culture with glucose or fructose as the sole carbon source compared with the group cultured in YEPD medium, the total number of peroxisomes showed no significant difference in either the hyphae or conidia at 6 and 9 hpi, but the number per unit length (0.1 mm) of hyphae was greater because the hyphae were shorter in the glucose or fructose medium than in the YEPD medium (Fig. 5a–c). Conversely, under culture with glucose or fructose as the sole carbon source, the number of AP-like structures formed by hyphae was significantly higher than that in YEPD medium (Fig. 5d). In particular, under culture in fructose, the number of AP-like structures was at least 5 times and twice as high as that under culture in YEPD medium and glucose, respectively. When oleic acid was used as the sole carbon source, the number of peroxisomes in the conidia, hyphae, and per unit hyphae increased significantly (Fig. 5a–c). Consistent with this, culturing in oleic acid compared with that in YEPD medium or in glucose also increased AP-like structure formation (Fig. 5d). Taken together, these results suggest that the increase in AP-like structure formation may be independent of peroxisome pathway activation in *B. cinerea* when cultured with sugars but may be positively correlated with peroxisome pathway activation in response to fatty acid induction.

The transcript levels of 6 DEGs annotated to the peroxisome pathway in mycelia of *B. cinerea* cultured in different media were evaluated by RT-qPCR. Most genes exhibited higher transcript levels in mycelia cultured in oleic acid at both time points (6 and 9 hpi) than those cultured in YEPD, glucose, or fructose (Fig. 5e). Onion epidermal cell infection experiments demonstrated that the hyphae were more likely to invade plant cells under culture conditions that facilitated the production of more AP-like structures (fructose > oleic acid > glucose) (Fig. 6a, b), consistent with the aforementioned result that more peroxisomes were produced in hyphae at the initial infection stage in the presence of oleic acid (Fig. 6c–e). Meanwhile, the transcript levels of these 6 DEGs in mycelia of *B. cinerea* collected from onion epidermal cells were higher than those in mycelia collected from cellophane (Fig. 6f).

### *B. cinerea* peroxisomes may function in response to extracellular stress

Peroxisome fission affects the cell wall integrity of *M. oryzae* (Chen et al. 2017). To test the responses of *B. cinerea* peroxisomes to different extracellular stresses, we cultured *B. cinerea* in the presence of different stress agents in YEPD medium, including the cell wall stressor Congo red (CR), the oxidative stressor $H_2O_2$, and biological stressors from the biocontrol bacterium *Bacillus velezensis* QSE-21 (Xu et al. 2021). These reagents inhibited the hyphal growth of *B. cinerea* to varying degrees at 6 and 9 hpi (Fig. 7a, b). Compared with the control group

(See figure on next page.)

**Fig. 2** Relative expression analysis of 12 DEGs during the early stage of *B. cinerea* infection via RT-qPCR. **a** Hierarchical cluster analysis of the indicated samples based on gene transcript levels. Each gene is represented by a single row of coloured boxes, and each small rectangle with different colours represents the log2 value of the relative gene expression level. **b** Comparison of gene expression levels with or without tomato leaf induction. The Y-axis represents the log2 value of the relative expression level. The expression level of each gene at conidial stage was set as '1' and used as sample control. *BcTubulin* was used as an endogenous control. The values represent the average values, and the error bars indicate the standard deviations of 3 technical replicates in one experiment. All experiments were repeated three times with consistent results

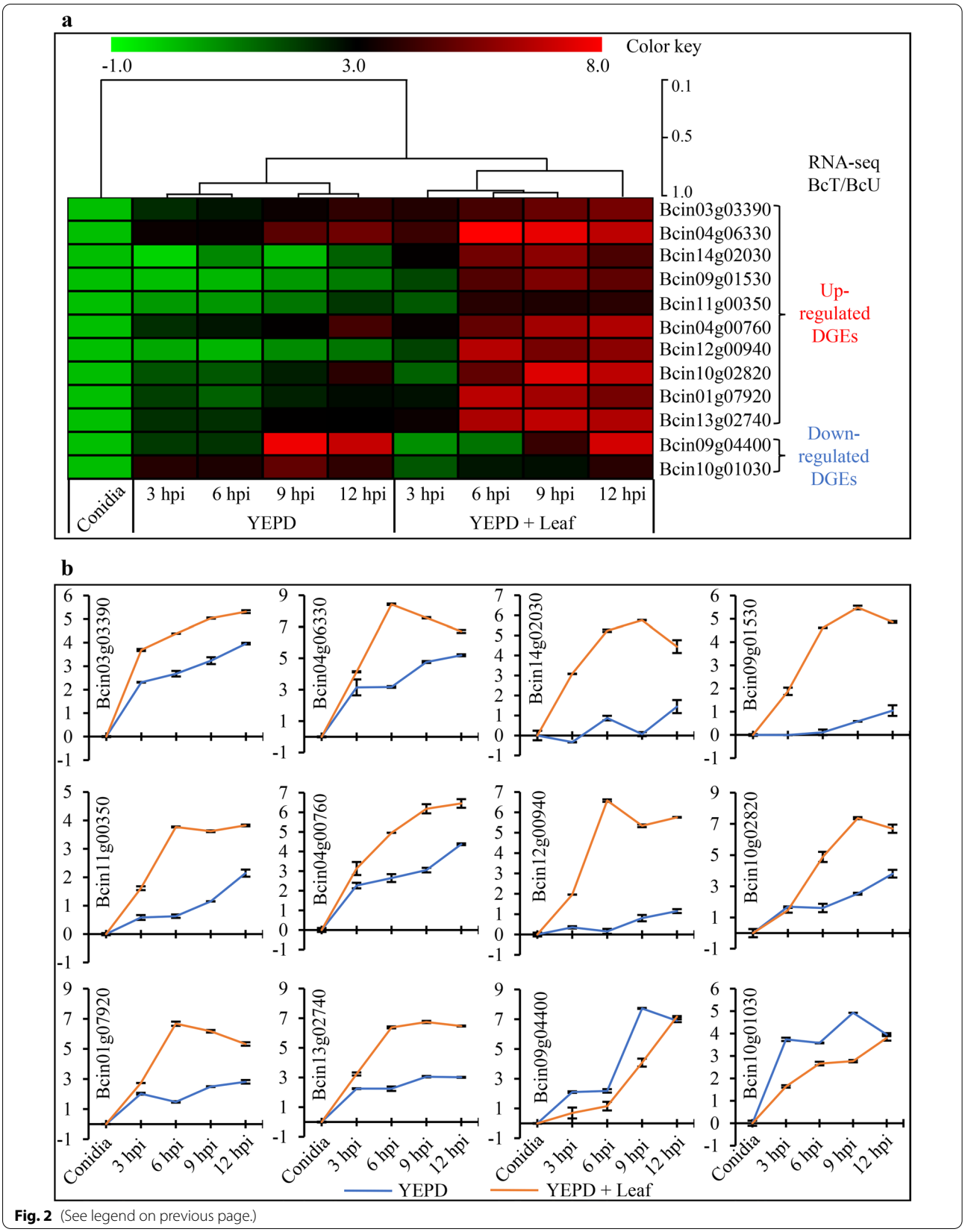


**Fig. 2** (See legend on previous page.)

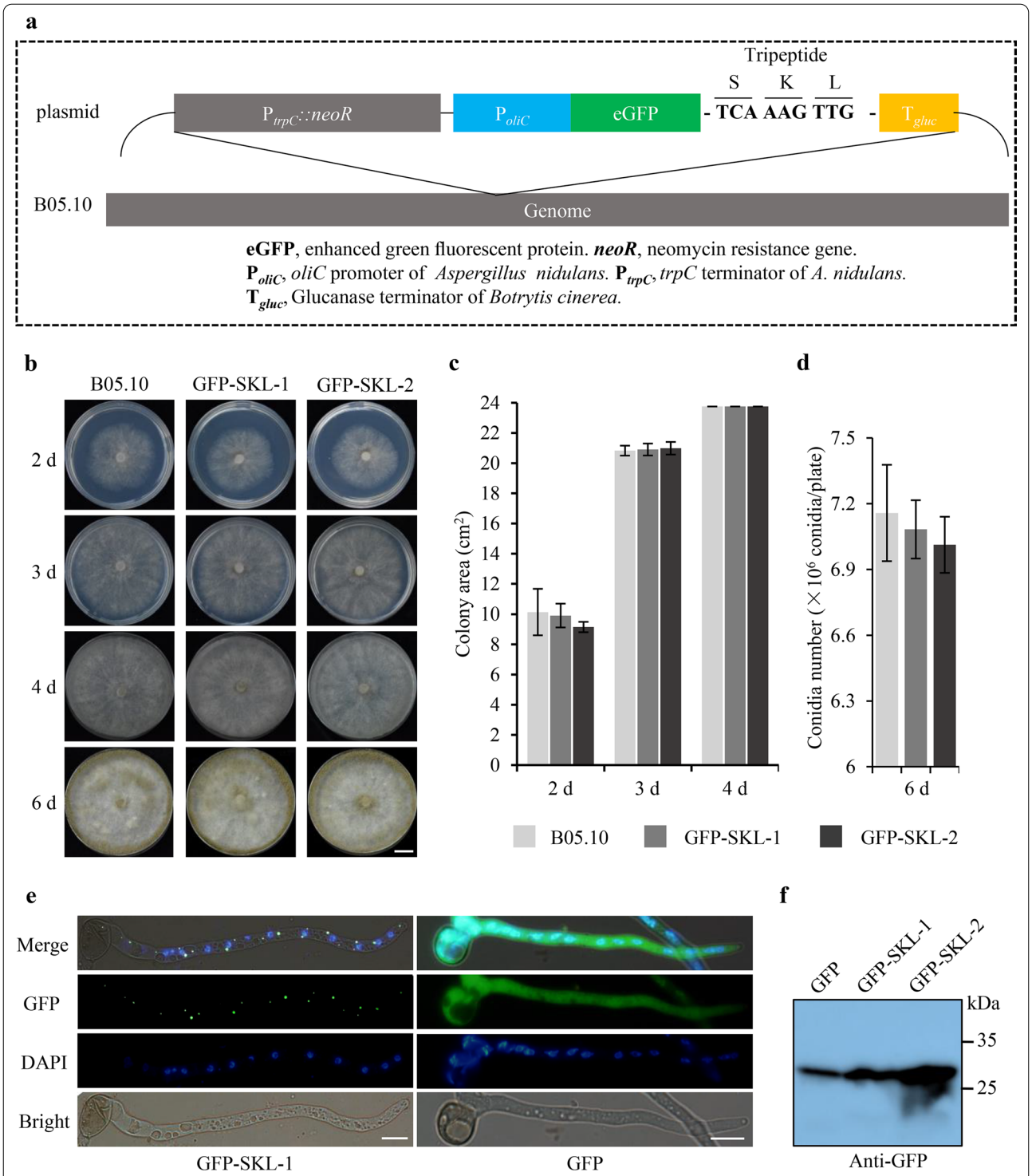


**Fig. 3** Construction and phenotype of a *B. cinerea* strain expressing a peroxisome-localized marker. **a** Schematic diagram of the gene overexpression plasmid used for transformation of the *B. cinerea* strain B05.10. **b** Growth phenotypes of the wild-type strain B05.10 and its derivatives containing GFP-SKL at the indicated times. Bar=1 cm. **c**, **d** Colony area and conidia number of strains B05.10 and GFP-SKL-1/2 at the indicated times. The values represent the average values, and the error bars indicate the standard deviations of three plates in one experiment. **e** Fluorescence signals produced by *B. cinerea* strains containing GFP-SKL or GFP only (GFP with no SKL tag). A fluorescence microscope with GFP channel and UV channel was used. Bar=10 μm. **f** Detection of GFP and GFP-SKL proteins expressed in *B. cinerea* by western blot assay using GFP antibody. All experiments were repeated three times with consistent results

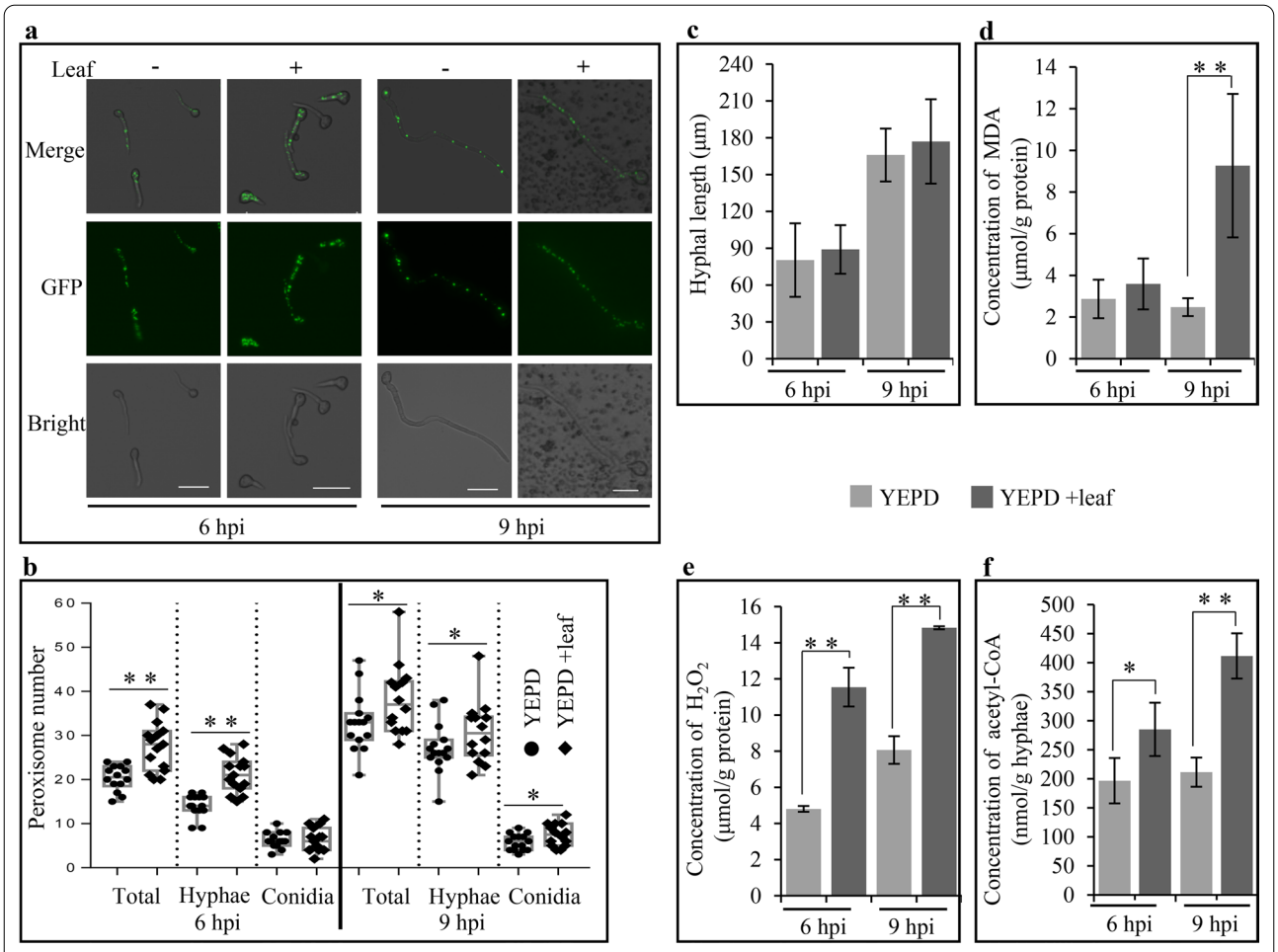


**Fig. 4** Induction with tomato leaves increases the number of peroxisomes in *B. cinerea* hyphae. **a** Fluorescence produced by strain GFP-SKL under a fluorescence microscope. Bar=50 μm. **b** Scatter plot showing the number of peroxisomes. **c** Column chart showing hyphal length. The values represent the average values, and the error bars indicate the standard deviations of 15 hyphae in one experiment. **d** Column chart showing the concentration of MDA per unit protein. **e** Column chart showing the concentration of $H_2O_2$ per unit protein. **f** Column chart showing the acetyl-CoA level per unit hyphae. In **d–f**, the values represent the average values, and the error bars indicate the standard deviations of 3 technical replicates in one experiment. *, $P<0.05$; **, $P<0.01$. All experiments were repeated three times with consistent results

cultured in YEPD medium without adding stress reagents, the number of peroxisomes produced in *B. cinerea* in response to these three stress reagents showed no significant difference in the conidia, a small increase in the hyphae at 9 hpi, and a significant increase in hyphae per unit length (Fig. 7a, c). Meanwhile, the transcript levels of the 6 DEGs annotated to the peroxisome pathway in *B. cinerea* cultured in YEPD medium or YEPD medium

(See figure on next page.)

**Fig. 5** Induction with exogenous oleic acid increases the number of peroxisomes in *B. cinerea* hyphae. **a** Fluorescence of *B. cinerea* strain GFP-SKL cultured in the indicated medium, including YEPD medium or medium with glucose, fructose, or oleic acid as the sole carbon source. Bar=50 μm. The red arrows indicate the AP-like structure. **b**, **c** Column charts showing the statistics of hyphal length and peroxisome number. The values represent the average values, and the error bars indicate the standard deviations of 20 hyphae in one experiment. **d** Column chart showing the statistics of the AP-like structures. The values represent the average values, and the error bars indicate the standard deviations of 3 groups of hyphae under microscopic fields in one experiment. Each group contained 3–4 independent microscopic fields, with a total of approximately 50 hyphae. **e** Relative expression level analysis of 6 DEGs annotated to the peroxisome pathway via RT-qPCR. *BcTubulin* was used as an endogenous control, and the sample collected from 10% YEPD medium at 6 hpi was used as a sample control. The values represent the average values, and the error bars indicate the standard deviations of 3 technical replicates in one experiment. The different letters (a, b, c, and d) indicate significant differences at the level of $P<0.01$. All experiments were repeated three times with consistent results

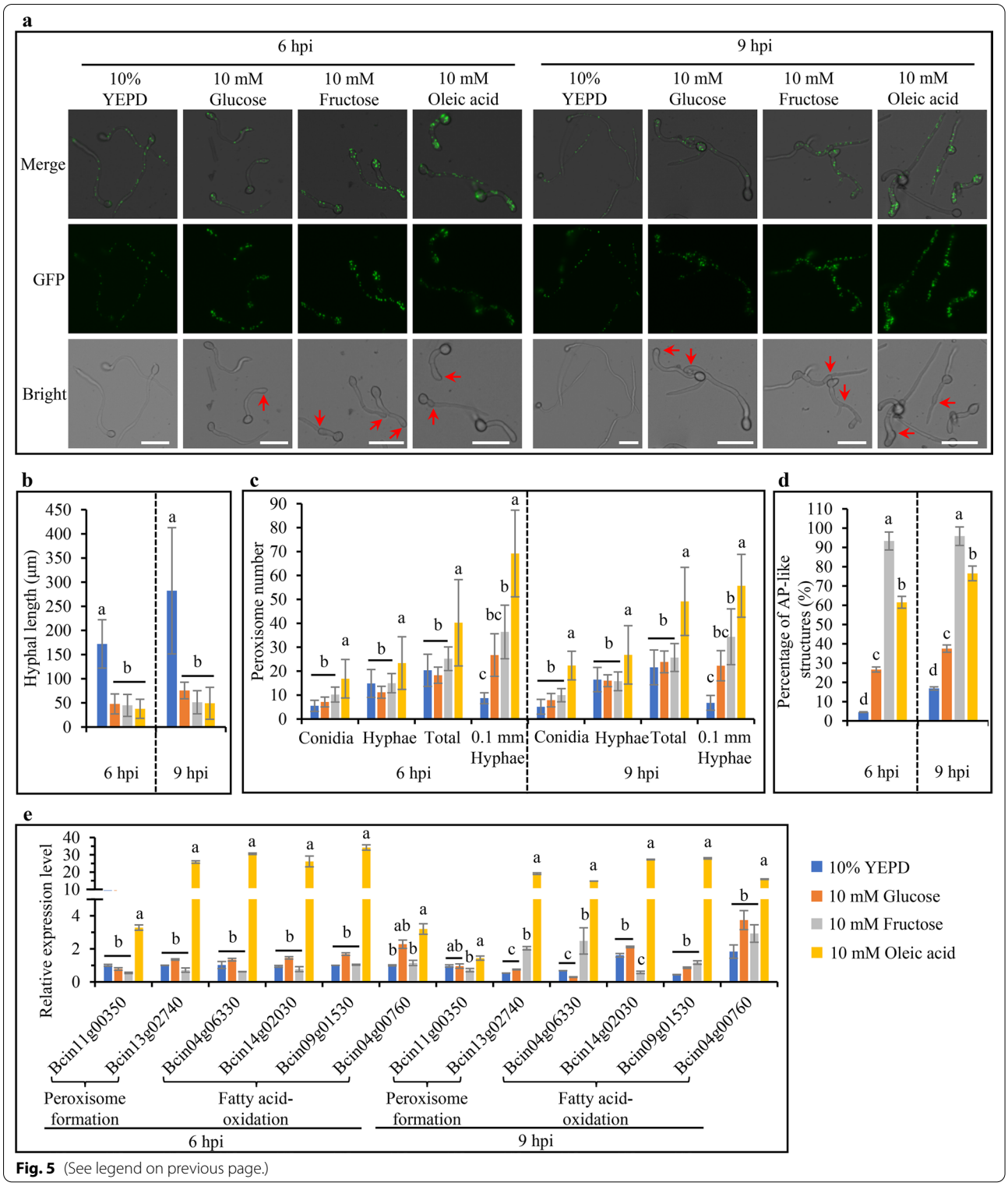


**Fig. 5** (See legend on previous page.)

containing QSE-21 were measured by RT-qPCR. The results showed that most of these genes were transcriptionally upregulated in response to QSE-21 (Fig. 7d), indicating that the peroxisome pathway in *B. cinerea* may be activated in response to various extracellular stressors.

## Discussion

Research on the functions of peroxisomes has been ongoing for decades, and peroxisomes are known to be widely involved in multiple biological processes. In recent years, studies have shown that peroxisomes are related to several human genetic diseases (Wanders 2013) and perform functions in pathogen–host plant interactions (Kubo 2013). In the present study, we found that approximately 52% (34/66) of the genes in the peroxisome pathway (bfu04146) were upregulated more than twofold at the initial stage of *B. cinerea* infection (Figs. 1, 2). We also observed that peroxisomal functions in *B. cinerea* can be enhanced by an increase in peroxisome number during the initial infection stage, during growth in medium with oleic acid as a sole carbon source or in onion epidermal cells, and in response to extracellular stress (Figs. 4–7). Interestingly, we found that the formation of AP-like structure and the ability of *B. cinerea* to penetrate plant cells when using oleic acid as the sole carbon source may be positively correlated with an increase in peroxisome number (Figs. 5, 6). These results indicated that lipid metabolism in peroxisomes plays important roles in *B. cinerea* initial infection.

Intracellular storage lipids, mainly triacylglycerols (TAGs), are universally used for energy storage in fungal conidia (Both et al. 2005; Ma et al. 2021), and the expression of lipid metabolism-related genes is strongly induced during infection of plant hosts by fungal pathogens (Chen et al. 2018; Lanver et al. 2018). TAGs can be transported from conidial cells to the incipient APs and then decomposed by intracellular lipases to release fatty acids and glycerol, after which the fatty acids can be metabolized through the peroxisome pathway, which is essential for turgor generation and appressorial penetration during fungal pathogen infection (Thines et al. 2000; Chen et al. 2017). In peroxisomes, fatty acid β-oxidation begins with a reaction catalysed by acyl-CoA oxidase (ACOX) and then by other multifunctional β-oxidation proteins, including 2-enoyl-CoA hydratase, 3-hydroxacyl-CoA dehydrogenase, and 3-ketoacyl-CoA thiolase; finally, a two-carbon unit acetyl-CoA is produced (Wang et al. 2007). In *M. oryzae*, MFP1, a protein that functions as a peroxisomal β-oxidation enzyme, and PTH2 and CRAT2, which function in acetyl-CoA transport, have been shown to play important roles in fatty acid metabolism and pathogenesis (Bhambra et al. 2006; Chen et al. 2016). The produced acetyl-CoA is then used for gluconeogenesis and synthesis of other metabolites, including polyketides, biotin, melanin, and cell wall components, in peroxisomes and other organelles (van der Klei and Veenhuis 2013; Chen et al. 2016).

The metabolism of intracellular fatty acids requires the peroxisome pathway, and exogenous addition of fatty acids can also induce the activation of the peroxisome pathway (Chen et al. 2017; Kong et al. 2019). Plant cell surfaces and intercellular spaces are rich in various lipids (Li et al. 2007; Keymer and Gutjahr 2018). Regardless of whether they synthesize fatty acids independently, both symbiotic and parasitic fungi in plants can exploit host lipids or lipid sources to sustain colonization or facilitate invasion (Jiang et al. 2017; Keymer and Gutjahr 2018). The assimilation of plant structural lipids by fungi benefits from multiple secreted lipases and phospholipases, which function as hydrolytic or lytic enzymes to degrade host waxes, cuticles, cell walls, and plasma membranes (Bravo-Ruiz et al. 2013). These extracellular lipolytic enzymes are associated with adhesion to and penetration of the plant surface by fungal pathogens and the generation of nutrients during certain stages of the fungal life cycle (Feng et al. 2009; Bravo-Ruiz et al. 2013; González et al. 2016). In *B. cinerea*, a secreted lipase, Lip1, has been identified and shown to be induced in the early stages of infection (Comménil et al. 1995; CommÉNil et al. 1999), but deletion of *Lip1* has no effect on the pathogenicity of the fungus on tomato and bean leaves (Reis et al. 2005). The function of host lipids and secreted lipases in the interaction of *B. cinerea* with its hosts therefore needs further investigation.

Oxidative reactions in peroxisomes are very important sources of intracellular ROS, mainly including superoxide radicals ($O_2^{\bullet-}$) and $H_2O_2$ (Sandalio et al. 2013; Chen et al. 2016). Peroxisomes are enriched with antioxidant enzymes, including superoxide dismutase

(See figure on next page.)

**Fig. 6** The invasive ability of *B. cinerea* is positively correlated with the activation of the peroxisome pathway. **a** *B. cinerea* hyphae in onion epidermal cells at 12 hpi after stained with trypan blue. Bar=100 μm. **b** Scatter plot showing the percentage of invasive hyphae in **a**. The different letters (a, b, and c) indicate significant differences at the level of $P<0.01$. **c** Fluorescence produced by strain GFP-SKL on onion epidermal layers. Bar=50 μm. **d**, **e** Column charts showing hyphal length and peroxisome number. In **b, d,** and **e**, the values represent the average values, and the error bars indicate the standard deviations of 20 images in one experiment. **f** Relative expression levels of 6 DEGs annotated to the peroxisome pathway. The onion epidermal cells or cellophane were inoculated with conidial droplets in 10 mM glucose, and then collected at the indicated times for RT-qPCR analysis. The Y-axis represents the log2 value of the relative expression level. The expression level of each gene in conidia was set as '1' and used as sample control. *BcTubulin* was used as an endogenous control. The values represent the average values, and the error bars indicate the standard deviations of 3 technical replicates in one experiment. All experiments were repeated three times with consistent results

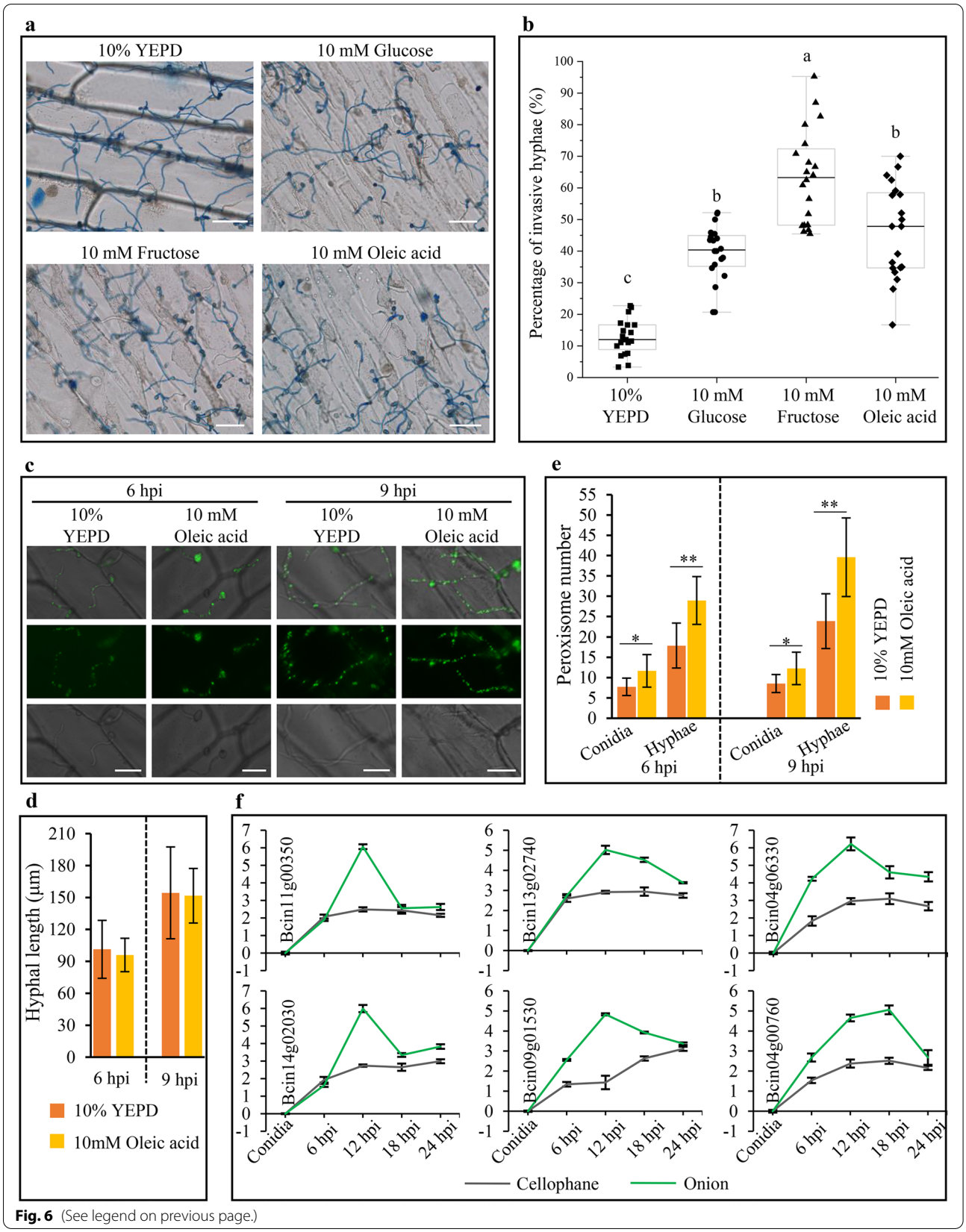


**Fig. 6** (See legend on previous page.)

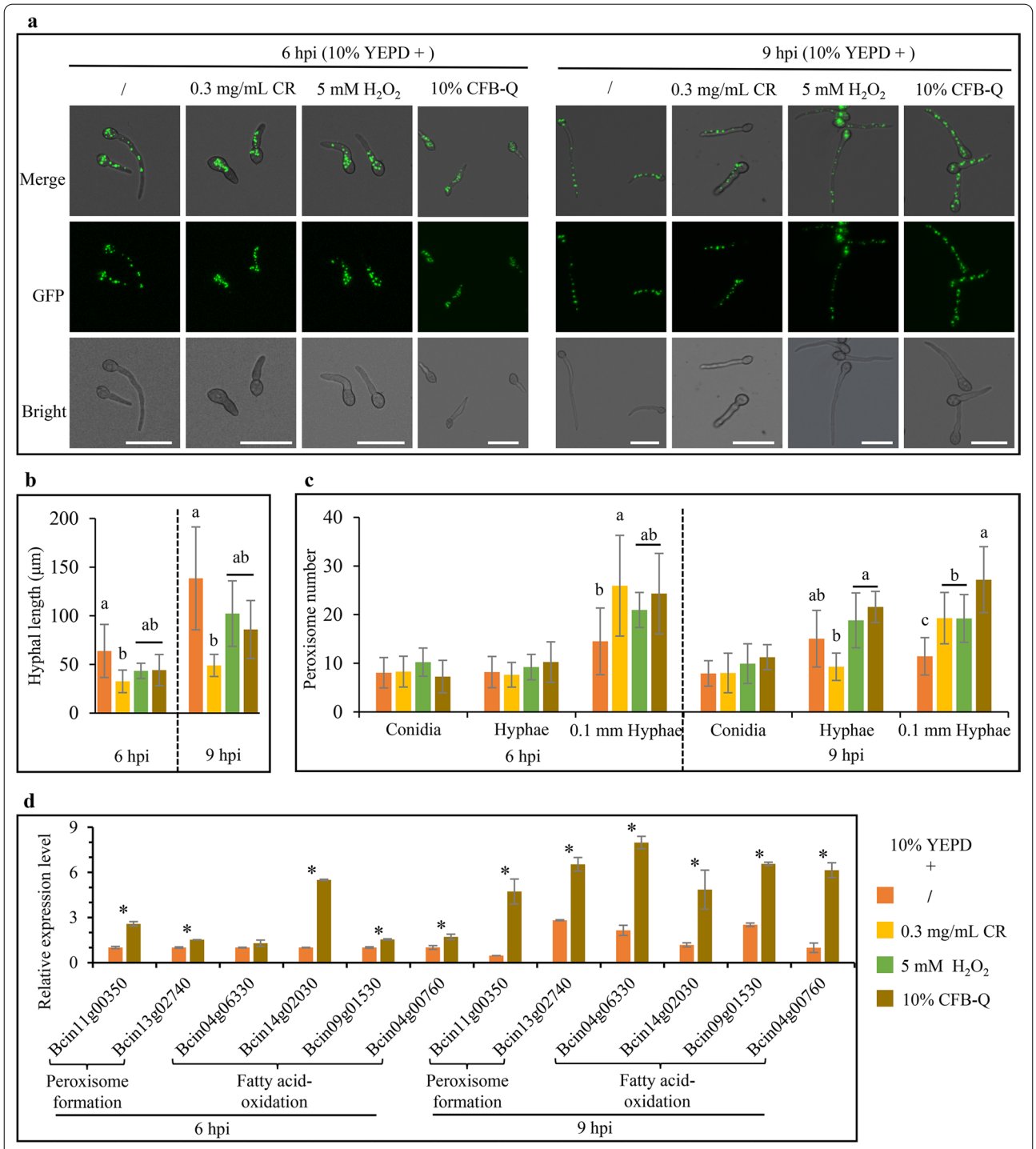


**Fig. 7** Induction with different stresses increases the number of peroxisomes in *B. cinerea* hyphae. **a** Fluorescence of *B. cinerea* strain GFP-SKL after incubation in 10% YEPD medium containing 0.3 mg/mL CR, 5 mM $H_2O_2$, or 10% cell-free fermentation broth of *B. velezensis* QSE-21 (CFB-Q). Bar = 50 μm. **b**, **c** Column charts showing hyphal length and peroxisome number. The values represent the average values, and the error bars indicate the standard deviations of 20 hyphae in one experiment. The different letters (a, b, and c) indicate significant differences at the level of $P < 0.01$. **d** Relative expression levels of 6 DEGs annotated to the peroxisome pathway via RT-qPCR analysis. *BcTubulin* was used as an endogenous control, and the sample collected from 10% YEPD medium at 6 hpi was used as a sample control. The values represent the average values, and the error bars indicate the standard deviations of 3 technical replicates of one experiment. *, $P < 0.01$

(SOD) and catalase; thus, excess ROS that are toxic to living cells can be rapidly scavenged in this organelle (Sandalio et al. 2013; Kong et al. 2019). Our results showed that the transcript level of a few catalase-coding genes was downregulated and that the $H_2O_2$ content increased at the initial stage of *B. cinerea* infection (Figs. 1, 4). This may be related to the dual function of ROS in mediating pathogen–host interactions. In *M. oryzae*-rice interactions, the accumulation of ROS is important for the AP development of the pathogen and for the host plant to initiate local programmed cell death to restrict the spread of invasive hyphae (Liu and Zhang 2021). When attacked by pathogens, plant hosts generally react with rapid and transient accumulation of ROS, referred to as an oxidative burst, to activate their defence system against pathogen invasion. However, the oxidative burst seems to be essential for successful infection by *B. cinerea* (Siegmund and Viefhues 2016). The absence of BcSOD1, a peroxisomal matrix protein, was shown to reduce the virulence of *B. cinerea* on different hosts (Rolke et al. 2004). BcSOD1 converts $O_2^{\bullet-}$ to $H_2O_2$, which can be used to damage plant tissues and attenuate the activation of plant defences (López-Cruz et al. 2017). This evidence indicates that the toxicity of $H_2O_2$ may be exploited by *B. cinerea* during infection, although thus far, it is difficult to discriminate whether $H_2O_2$ is secreted by *B. cinerea* or produced by *B. cinerea*-infected host plants (López-Cruz et al. 2017).

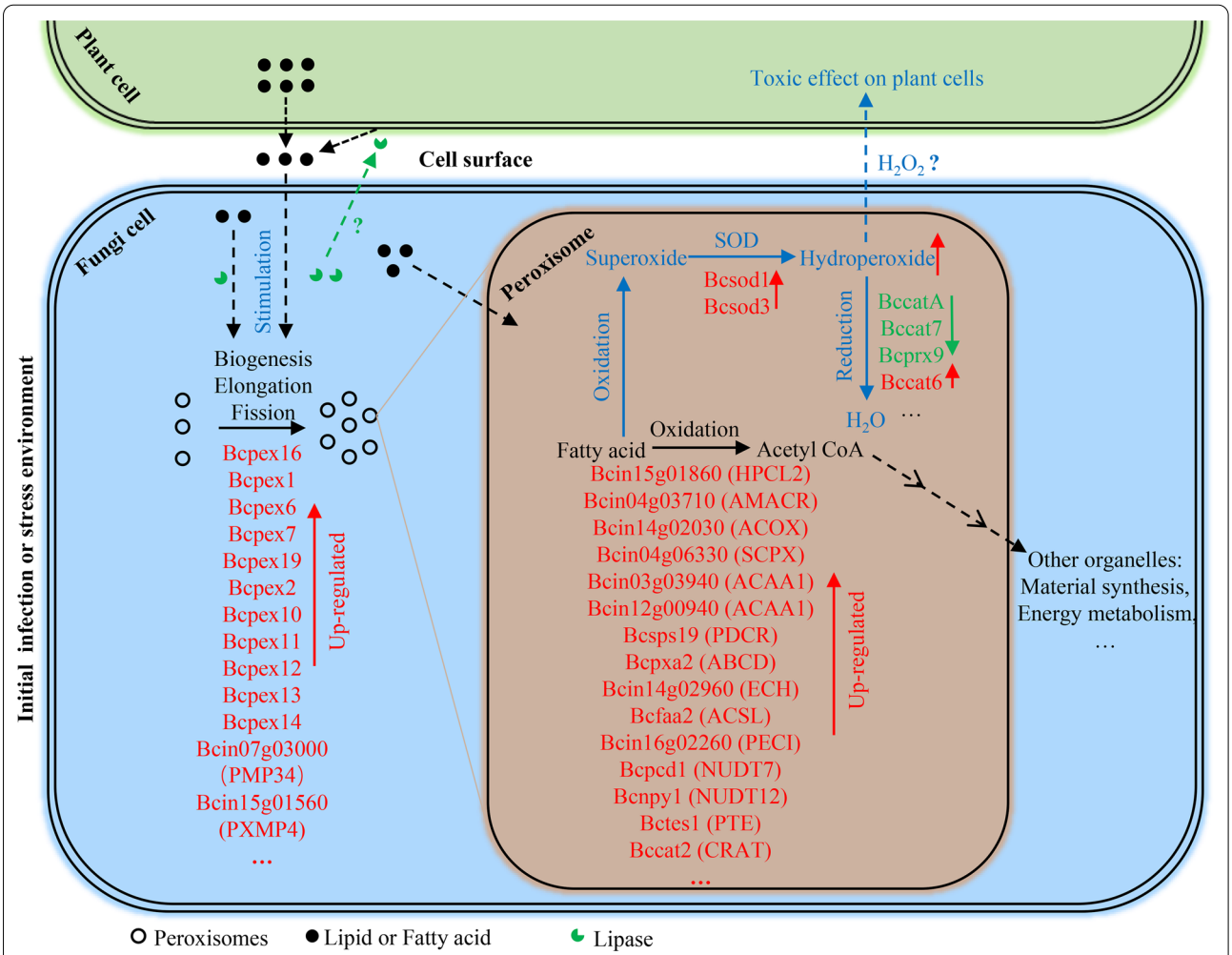


**Fig. 8** Working model of fatty acid oxidation in peroxisomes during the initial stage of *B. cinerea* infection. The contents in brackets represent the symbols according to the KEGG results. ABCD, ATP-binding cassette, subfamily D; ACAA, Acetyl-CoA acyltransferase; ACOX, Acyl-CoA oxidase; ACSL, Long-chain acyl-CoA synthetase; AMACR, α-methylacyl-CoA racemase; CAT, Catalase; CRAT, Carnitine O-acetyltransferase; ECH, δ(3,5)-δ(2,4)-dienoyl-CoA isomerase; HPCL, 2-hydroxyacyl-CoA lyase; NUDT, Diphosphatase; PDCR, 2,4-dienoyl-CoA reductase; PECI, δ(3)-δ(2)-enoyl-CoA isomerase; pex, Peroxin; PMP and PXMP, Peroxisomal membrane protein; PTE, Acyl-CoA thioesterase; SCPX, Sterol carrier protein; SOD, Superoxide dismutase

## Conclusions

In summary, the working model of peroxisomal metabolism in *B. cinerea* during the initial stage of infection or in response to stress is shown in Fig. 8. The metabolism of intracellular or extracellular host lipids increases via stimulation of peroxisome proliferation. Accompanying the oxidation of fatty acids in peroxisomes, a large amount of acetyl-CoA is produced, which can be used to synthesize other compounds, form infection structures or cope with stress; and a high level of $H_2O_2$ is accumulated, which may be used to damage host tissues. Of course, there remain many issues that need to be addressed in future research, such as how *B. cinerea* uses host lipids to complete infection, how excessive $H_2O_2$ is transported to host cells, and how the expression of genes involved in peroxisome formation and matrix metabolism is coordinated. As the peroxisome pathway may play important roles in the initial stage of infection by fungal pathogens, the key proteins in this pathway may be good targets for the development of new fungicides.

## Methods

### Bioinformatics analysis of DEGs annotated to the peroxisome pathway

In the genome of *B. cinerea*, a total of 66 genes were annotated to the peroxisome pathway (bfu04146: https://www.kegg.jp/pathway/bfu04146) in the KEGG database. These 66 genes were used to search a transcriptome sequencing data of *B. cinerea* mycelia collected from medium with or without tomato leaves induction (BcT or BcU) at 6 hpi, which has been deposited in NCBI Sequence Read Archive (SRA) with an accession number PRJNA837395. The transcriptome data contained 2,975 DEGs listed in Additional file 1: Table S4 with a threshold of $P$ value < 0.05 and fold-change ≥ 2. Hierarchical clustering of DEGs annotated to the peroxisome pathway was performed using Multiexperimental Viewer (MeV) software (Saeed et al. 2006) according to their expression patterns from the transcriptome data with three biological replicates or from RT-qPCR results. GO annotation was implemented on the online server QuickGo (https://www.ebi.ac.uk/QuickGO/), and the genes were classified by GO annotation based on the categories: biological process, cellular component, and molecular function. Protein sequences, encoded by DEGs annotated into peroxisome pathway, were downloaded from the *B. cinerea* genome database (ASM83294v1) in EnsemblFungi (http://fungi.ensembl.org/Botrytis_cinerea/Info/Index). And then sequences were used to blast the PHI database (http://www.phi-base.org/) (Urban et al. 2020) with an e-value < 1E-5 cut-off as previously mentioned (Bashyal et al. 2017). PPI analysis was performed using the Search Tool for the Retrieval of Interacting Genes/Proteins (STRING version 11.5, https://cn.string-db.org/) with a confidence score larger than 0.4 and clustered by the MCL algorithm.

### RNA extraction and RT-qPCR

The mycelia cultured under the above-mentioned conditions was collected by centrifugation and blotted dry with filter paper. Total RNA was extracted from mycelia or conidia using the OMEGA fungal RNA kit (E.Z.N.A. R6840), and 1 μg of total RNA of each sample was used for the first strand cDNA synthesis using the M5 Super plus qPCR RT kit with gDNA remover (Mei5bio, MF166-plus). qPCR was performed on a LightCycler 96 instrument (Roche, Mannheim, Germany) using 2 × M5 HiPer Real-time PCR Super Mix (Mei5bio, MF797) according to the manufacturer's instructions. The transcriptional level of genes was calculated according to the $2^{-\Delta\Delta Cq}$ method (Livak and Schmittgen 2001) using *B. cinerea* tubulin gene (*BcTubulin*, Bcin01g08040) as endogenous reference. Primers used for qPCR were designed by Beacon Designer 8 software and were listed in Additional file 1: Table S5.

### Fungal strains and culture conditions

The wild-type strain B05.10 of *B. cinerea* and its derivative transformants were grown and maintained on PDA medium (200 g potato, 20 g glucose, 15 g agar, and 1 L water) under conditions as described previously (Giesbert et al. 2011). To mimic the initial stage of infection, conidia suspension of *B. cinerea* were inoculated into 10% YEPD liquid medium (10 g yeast extract, 20 g peptone, 20 g glucose, and 1 L water) supplemented with 3-week-old tomato leaves (about 20 g leaves per 100 mL) and cultured on a rotary shaker at 25 ℃ and 120 rpm. The single carbon source tests were performed in minimal liquid medium (MM: 0.5% $(NH_4)_2SO_4$, 0.1% $KH_2PO_4$, 0.05% $MgSO_4$) supplemented with glucose, fructose, or oleic acid at a final concentration of 10 mM under the above-mentioned conditions. To simulate the extracellular stress, conidia of *B. cinerea* were inoculated into 10% YEPD liquid medium and cultured on a rotary shaker at 25 ℃ and 180 rpm for 3 h, followed by adding CR (final concentration 0.3 mg/mL), $H_2O_2$ (final concentration 5 mM), or cell free fermentation broth of *Bacillus velezensis* QSE-21 (CFB-Q) (final concentration 10%), and then were incubated for another 3 h or 6 h. The CFB-Q was prepared as described previously (Xu et al. 2021). *B. cinerea* conidia harvested from 7-day-old PDA plate was suspended in the above-mentioned liquid medium at a final concentration of $1 \times 10^5$ conidia/mL.

### Generation of GFP-SKL labelled *B. cinerea* strains and fungal development assays

The coding sequence of the tripeptide 'SKL', TCAAAG TTG, was added to the 3` end of GFP sequence by PCR using primers listed in Additional file 1: Table S5. PCR product was then ligated into the *NcoI*/*NotI*-digested pNDT-OGG vector (Schumacher 2012). Protoplast preparation and transformation were performed as described previously (Gronover et al. 2001). The resulting hygromycin-resistant transformants were preliminarily validated by PCR followed by several rounds of single conidium isolation. Fungal growth and conidiation assays on PDA were performed as described previously (Feng et al. 2017).

### Western blot analysis

*B. cinerea* conidia harvested from 7-day-old PDA plates were inoculated in YEPD medium and cultured on a rotary shaker at 25 ℃ and 180 rpm for 16 h. The mycelia were harvested by filtration through filter paper and washed several times with sterile distilled water. Total proteins were extracted from mycelia as described previously (Gu et al. 2015). Equal volume of protein samples was loaded and separated on 12% sodium dodecylsulphate-polyacrylamide gel electrophoresis (SDS-PAGE), and then transferred to polyvinylidene fluoride (PVDF) membrane with a Bio-Rad electroblotting apparatus. The anti-GFP antibody (Abcam, Cambridge, Cat#Ab32146) was used to detect GFP and GFP-SKL protein. The experiment was performed three times independently.

### Microscopic examinations

For the observation of GFP signal, fresh hyphae cultured in different liquid media were transferred to a glass slide and then examined with a fluorescence microscope under the GFP channel. For the observation of nuclei in hyphae, fresh hyphae were stained with 10 μg/mL of DAPI and then examined with a fluorescence microscope under the UV channel. The morphology of hyphae was examined in the bright field. The number of fluorescent spots was counted and the length of fungal hyphae was measured using ImageJ software from images taken under the same conditions.

For AP-like structure formation assay, 20 μL-droplets of conidial suspension ($1\times10^5$ conidia/mL) were placed onto a glass slide and incubated in a moistened box at 25 °C. The proportion of AP-like formation inoculated into different media was determined by microscopic examination as described previously (Feng et al. 2017). The infection assay in onion epidermal cells was performed as described previously using conidial droplets ($1\times10^4$ conidia/mL) suspended in different media. The proportion of invasive hyphae to total conidia in each image was determined using ImageJ software.

### Detection of lipid β-oxidation level, $H_2O_2$ content and acetyl-CoA level

Mycelia cultured in liquid medium was collected by centrifugation and blotted dry with filter paper. An amount of 0.1 g mycelia was homogenized in a glass tissue homogenizer containing 1 mL of ice-cold PBS buffer (8.0 g NaCl, 0.2 g KCl, 1.44 g $Na_2HPO_4$, 0.24 g $KH_2PO_4$, 1 L $H_2O$). The homogenate was transferred to a tube followed by centrifuging for 10 min at $12,000\times g$ at 4 °C and then the supernatant was transferred to a new tube and kept at 4 °C before use. Lipid β-oxidation level was then determined by detecting the content of MDA using a Lipid Peroxidation MDA Assay Kit (Beyotime, S0131S) based on thiobarbituric acid (TBA) test (Heath and Packer 1968). Measurement of $H_2O_2$ content was carried out using a Hydrogen Peroxide Assay Kit (Beyotime, S0038) based on the Ferric Xylenol Orange method (Gay et al. 1999). The measurement of acetyl-CoA level was carried out using an Acetyl-CoA Content Assay Kit (Solarbio, BC0980) based on the formation rate of NADH, which is directly proportional to the acetyl-CoA level through the coupled reaction between malate dehydrogenase and citrate synthase. And the quantification of NADH was further carried out by spectrophotometry. For comparison between samples, the concentration of MDA and $H_2O_2$ was normalized with the protein concentration in the sample and expressed as μmol/g protein. The protein concentration was determined using BCA method performed by a BCA Protein Assay Kit (Beyotime, P0012S). Three biological replicates for each experiment and three technical replicates for each biological replicate were performed.

### Statistical analysis

All data were expressed as the means ± standard deviations obtained from more than three replicates per experimental condition. The least significant differences (LSD) method for multiple comparisons was carried out with Statistical Analysis Systems (SAS) software to determine differences between means.

#### Abbreviations

acetyl-CoA: Acetyl-coenzyme A; ACOX: Acyl-CoA oxidase; AP: Appressorium; CFB-Q: Cell free fermentation broth of *Bacillus velezensis* QSE-21; CoA: Coenzyme A; CR: Congo red; CRAT2: Carnitine O-acetyltransferase 2; DAPI: 4′,6-Diamidino-2-phenylindole; DEGs: Differentially expressed genes; FC: Fold change; FPKM: Fragments per kilobase of exon per million fragments mapped; GFP: Green fluorescent protein; GO: Gene ontology; $H_2O_2$: Hydrogen peroxide; hpi: Hours post-inoculation; KEGG: Kyoto Encylcopedia of Genes and Genomes; LSD: Least significant differences; MCL: Markov cluster; MDA: Malondialdehyde; MeV: Multiexperimental viewer; MFP1: Multifunctional protein 1; MM: Minimal medium; NADH: Nicotinamide adenine dinucleotide; NCBI:

National Center for Biotechnology Information; $O_2^{\bullet-}$: Superoxide radicals; PBS: Phosphate buffer saline; PDA: Potato dextrose agar; PEX: Peroxins; PHI: Pathogen–host interaction; PPI: Protein–protein interaction; PTS: Peroxisomal targeting signal; PVDF: Polyvinylidene fluoride; RT-qPCR: Reverse transcription-quantitative PCR; ROS: Reactive oxygen species; SAS: Statistical analysis system; SDS-PAGE: Sodium dodecylsulphate-polyacrylamide gel electrophoresis; SOD: Superoxide dismutase; SRA: Sequence read archive; STRING: Search tool for the retrieval of interacting genes/proteins; TAGs: Triacylglycerols; TBA: Thiobarbituric acid; WBs: Woronin bodies; YEPD: Yeast extract peptone dextrose.

## Supplementary Information

The online version contains supplementary material available at https://doi.org/10.1186/s42483-022-00130-4.

**Additional file 1: Table S1.** Detailed information of DEGs annotated to *B. cinerea* peroxisome pathway. **Table S2.** Details of GO terms of the DEGs annotated to *B. cinerea* peroxisome pathway. **Table S3.** Detailed information of PHI BLAST. **Table S4.** Information of total DEGs from a data of RNA-Seq. **Table S5.** Primers used in this study.

**Additional file 2: Fig. S1.** Bioinformatic analysis of the DEGs annotated to the peroxisome pathway in *B. cinerea* (KEGG pathway: bfu04146). **Fig. S2.** Induction with Tween-80 increases the number of fluorescent punctate structures.

**Acknowledgements**
Not applicable.

**Author contributions**
ML and WL designed the project, HH performed the experiments, HH and XN analysed the data. ML wrote the manuscript and WL revised the manuscript. All authors read and approved the final manuscript.

**Funding**
This research was supported by the Shandong Provincial Natural Science Foundation (ZR2020KC003), the Key Research and Development Program of Shandong Province (2019YQ017), Shandong Province 'Double-Hundred Talent Plan' (WST2018008), Taishan Scholar Construction Foundation of Shandong Province (TSHW20130963), and the Scientific Research Fund for High-Level Talents in Qingdao Agricultural University (20210036).

**Availability of data and materials**
The datasets generated and analysed during the current study are available in the NCBI repository [https://dataview.ncbi.nlm.nih.gov/object/PRJNA837395].

## Declarations

**Ethics approval and consent to participate**
Not applicable.

**Consent for publication**
Not applicable.

**Competing interests**
The authors declare that they have no competing interests.

Received: 14 March 2022 Accepted: 28 June 2022
Published online: 11 July 2022

**References**

Asakura M, Yoshino K, Hill AM, Kubo Y, Sakai Y, Takano Y. Primary and secondary metabolism regulates lipolysis in appressoria of *Colletotrichum orbiculare*. Fungal Genet Biol. 2012;49:967–75. https://doi.org/10.1016/j.fgb.2012.08.009.

Bashyal BM, Rawat K, Sharma S, Kulshreshtha D, Gopala Krishnan S, Singh AK, et al. Whole genome sequencing of *Fusarium fujikuroi* provides insight into the role of secretory proteins and cell wall degrading enzymes in causing bakanae disease of rice. Front Plant Sci. 2017;8:2013. https://doi.org/10.3389/fpls.2017.02013.

Bhambra GK, Wang ZY, Soanes DM, Wakley GE, Talbot NJ. Peroxisomal carnitine acetyl transferase is required for elaboration of penetration hyphae during plant infection by *Magnaporthe grisea*. Mol Microbiol. 2006;61:46–60. https://doi.org/10.1111/j.1365-2958.2006.05209.x.

Both M, Csukai M, Stumpf MPH, Spanu PD. Gene expression profiles of *Blumeria graminis* indicate dynamic changes to primary metabolism during development of an obligate biotrophic pathogen. Plant Cell. 2005;17:2107–22. https://doi.org/10.1105/tpc.105.032631.

Bravo RG, Ruiz RC, Roncero MI. Lipolytic system of the tomato pathogen Fusarium oxysporum f. sp. lycopersici. Mol Plant Microbe Interact. 2013;26:1054–67. https://doi.org/10.1094/mpmi-03-13-0082-r.

Chatzidimopoulos M, Psomopoulos F, Malandrakis EE, Ganopoulos I, Madesis P, Vellios EK, et al. Comparative genomics of *Botrytis cinerea* strains with differential multi-drug resistance. Front Plant Sci. 2016;7:554. https://doi.org/10.3389/fpls.2016.00554.

Chen XL, Shen M, Yang J, Xing Y, Chen D, Li Z, et al. Peroxisomal fission is induced during appressorium formation and is required for full virulence of the rice blast fungus. Mol Plant Pathol. 2017;18:222–37. https://doi.org/10.1111/mpp.12395.

Chen XL, Wang Z, Liu C. Roles of Peroxisomes in the rice blast fungus. Biomed Res Int. 2016;2016:9343417. https://doi.org/10.1155/2016/9343417.

Chen Y, Zheng S, Ju Z, Zhang C, Tang G, Wang J, et al. Contribution of peroxisomal docking machinery to mycotoxin biosynthesis, pathogenicity and pexophagy in the plant pathogenic fungus *Fusarium graminearum*. Environ Microbiol. 2018;20:3224–45. https://doi.org/10.1111/1462-2920.14291.

CommÉNil P, Belingheri L, Bauw G, Dehorter B. Molecular characterization of a lipase induced in *Botrytis cinerea* by components of grape berry cuticle. Physiol Mol Plant Pathol. 1999;55:37–43. https://doi.org/10.1006/pmpp.1999.0206.

Comménil P, Belingheri L, Sancholle M, Dehorter B. Purification and properties of an extracellular lipase from the fungus *Botrytis cinerea*. Lipids. 1995;30:351–6. https://doi.org/10.1007/BF02536044.

Dean R, Van Kan JA, Pretorius ZA, Hammond-Kosack KE, Di Pietro A, Spanu PD, et al. The Top 10 fungal pathogens in molecular plant pathology. Mol Plant Pathol. 2012;13:414–30. https://doi.org/10.1111/j.1364-3703.2011.00783.x.

Distel B, Erdmann R, Gould SJ, Blobel G, Crane DI, Cregg JM, et al. A unified nomenclature for peroxisome biogenesis factors. J Cell Biol. 1996;135:1–3. https://doi.org/10.1083/jcb.135.1.1.

Elad Y, Pertot I, Cotes Prado AM, Stewart A. Plant hosts of *Botrytis* spp. In: Fillinger S, Elad Y, editors. Botrytis - the fungus, the pathogen and its management in agricultural systems. Cham: Springer International Publishing; 2016a. p. 413–86. https://doi.org/10.1007/978-3-319-23371-0_20.

Elad Y, Vivier M, Fillinger S. *Botrytis*, the good, the bad and the ugly. In: Fillinger S, Elad Y, editors. *Botrytis* - the fungus, the pathogen and its management in agricultural systems. Cham: Springer International Publishing; 2016b. p. 1–15. https://doi.org/10.1007/978-3-319-23371-0_1.

Feng HQ, Li GH, Du SW, Yang S, Li XQ, de Figueiredo P, et al. The septin protein Sep4 facilitates host infection by plant fungal pathogens via mediating initiation of infection structure formation. Environ Microbiol. 2017;19:1730–49. https://doi.org/10.1111/1462-2920.13613.

Feng J, Wang F, Liu G, Greenshields D, Shen W, Kaminskyj S, et al. Analysis of a *Blumeria graminis*-secreted lipase reveals the importance of host epicuticular wax components for fungal adhesion and development. Mol Plant Microbe Interact. 2009;22:1601–10. https://doi.org/10.1094/mpmi-22-12-1601.

Fillinger S, Walker AS. Chemical control and resistance management of *Botrytis* diseases. In: Fillinger S, Elad Y, editors. *Botrytis* - the fungus, the pathogen and its management in agricultural systems. Cham: Springer International Publishing; 2016. p. 189–216. https://doi.org/10.1007/978-3-319-23371-0_10.

Fujihara N, Sakaguchi A, Tanaka S, Fujii S, Tsuji G, Shiraishi T, et al. Peroxisome Biogenesis factor PEX13 is required for appressorium-mediated plant infection by the anthracnose fungus *Colletotrichum orbiculare*. Mol Plant Microbe Interact. 2010;23:436–45. https://doi.org/10.1094/MPMI-23-4-0436.

Gay C, Collins J, Gebicki JM. Hydroperoxide assay with the ferric-xylenol orange complex. Anal Biochem. 1999;273:149–55. https://doi.org/10.1006/abio.1999.4208.

Giesbert S, Schumacher J, Kupas V, Espino J, Segmüller N, Haeuser-Hahn I, et al. Identification of pathogenesis-associated genes by T-DNA mediated insertional mutagenesis in *Botrytis cinerea*: A type 2A phosphoprotein phosphatase and an SPT3 transcription factor have significant impact on virulence. Mol Plant Microbe Interact. 2011;25:481–95. https://doi.org/10.1094/MPMI-07-11-0199.

González C, Brito N, Sharon A. Infection process and fungal virulence factors. In: Fillinger S, Elad Y, editors. *Botrytis* - the fungus, the pathogen and its management in agricultural systems. Cham: Springer International Publishing; 2016. p. 229–46.

Gronover CS, Kasulke D, Tudzynski P, Tudzynski B. The role of G protein alpha subunits in the infection process of the gray mold fungus *Botrytis cinerea*. Mol Plant Microbe Interact. 2001;14:1293–302. https://doi.org/10.1094/MPMI.2001.14.11.1293.

Gu Q, Zhang C, Liu X, Ma Z. A transcription factor FgSte12 is required for pathogenicity in *Fusarium graminearum*. Mol Plant Pathol. 2015;16:1–13. https://doi.org/10.1111/mpp.12155.

Heath RL, Packer L. Photoperoxidation in isolated chloroplasts. I. Kinetics and stoichiometry of fatty acid peroxidation. Arch Biochem Biophys. 1968;125:189–98. https://doi.org/10.1016/0003-9861(68)90654-1.

Hu MJ, Cox KD, Schnabel G. Resistance to increasing chemical classes of fungicides by virtue of "selection by association" in *Botrytis cinerea*. Phytopathology. 2016;106:1513–20. https://doi.org/10.1094/PHYTO-04-16-0161-R.

Islinger M, Voelkl A, Fahimi HD, Schrader M. The peroxisome: an update on mysteries 2.0. Histochem Cell Biol. 2018;150:443–71. https://doi.org/10.1007/s00418-018-1722-5.

Jiang Y, Wang W, Xie Q, Liu N, Liu L, Wang D, et al. Plants transfer lipids to sustain colonization by mutualistic mycorrhizal and parasitic fungi. Science. 2017;356:1172–5. https://doi.org/10.1126/science.aam9970.

Keymer A, Gutjahr C. Cross-kingdom lipid transfer in arbuscular mycorrhiza symbiosis and beyond. Curr Opin Plant Biol. 2018;44:137–44. https://doi.org/10.1016/j.pbi.2018.04.005.

Kimura A, Takano Y, Furusawa I, Okuno T. Peroxisomal metabolic function is required for appressorium-mediated plant infection by *Colletotrichum lagenarium*. Plant Cell. 2001;13:1945–57. https://doi.org/10.1105/tpc.010084.

Knoblach B, Sun X, Coquelle N, Fagarasanu A, Poirier RL, Rachubinski RA. An ER-peroxisome tether exerts peroxisome population control in yeast. EMBO J. 2013;32:2439–53. https://doi.org/10.1038/emboj.2013.170.

Kong X, Zhang H, Wang X, van der Lee T, Waalwijk C, van Diepeningen A, et al. FgPex3, a peroxisome biogenesis factor, is involved in regulating vegetative growth, conidiation, sexual development, and virulence in *Fusarium graminearum*. Front Microbiol. 2019;10:2088. https://doi.org/10.3389/fmicb.2019.02088.

Kubo Y. Function of peroxisomes in plant-pathogen interactions. In: del Río LA, editor. Peroxisomes and their key role in cellular signaling and metabolism. Netherlands Dordrecht: Springer; 2013. p. 329–45. https://doi.org/10.1007/978-94-007-6889-5_18.

Lanver D, Müller AN, Happel P, Schweizer G, Haas FB, Franitza M, et al. The biotrophic development of *Ustilago maydis* studied by RNA-Seq analysis. Plant Cell. 2018;30:300–23. https://doi.org/10.1105/tpc.17.00764.

Li Y, Beisson F, Ohlrogge J, Pollard M. Monoacylglycerols are components of root waxes and can be produced in the aerial cuticle by ectopic expression of a suberin-associated acyltransferase. Plant Physiol. 2007;144:1267–77. https://doi.org/10.1104/pp.107.099432.

Liu JK, Chang HW, Liu Y, Qin Y, Ding YH, Wang L, et al. The key gluconeogenic gene PCK1 is crucial for virulence of *Botrytis cinerea* via initiating its conidial germination and host penetration. Environ Microbiol. 2018;20:1794–814. https://doi.org/10.1111/1462-2920.14112.

Liu X, Zhang Z. A double-edged sword: reactive oxygen species (ROS) during the rice blast fungus and host interaction. The FEBS J. 2021. https://doi.org/10.1111/febs.16171.

Livak KJ, Schmittgen TD. Analysis of relative gene expression data using real-time quantitative PCR and the $2^{-\Delta\Delta CT}$ method. Methods. 2001;25:402–8. https://doi.org/10.1006/meth.2001.1262.

López-Cruz J, Óscar CS, Emma FC, Pilar GA, Carmen GB. Absence of Cu-Zn superoxide dismutase BCSOD1 reduces *Botrytis cinerea* virulence in Arabidopsis and tomato plants, revealing interplay among reactive oxygen species, callose and signalling pathways. Mol Plant Pathol. 2017;18:16–31. https://doi.org/10.1111/mpp.12370.

Ma H, Wu X, Wei Z, Zhao L, Li Z, Liang Q, et al. Functional divergence of diacylglycerol acyltransferases in the unicellular green alga *Haematococcus pluvialis*. J Exp Bot. 2021;72:510–24. https://doi.org/10.1093/jxb/eraa451.

Min K, Son H, Lee J, Choi GJ, Kim JC, Lee YW. Peroxisome function is required for virulence and survival of *Fusarium graminearum*. Mol Plant Microbe Interact. 2012;25:1617–27. https://doi.org/10.1094/mpmi-06-12-0149-r.

Miret JA, Munné-Bosch S, Dijkwel PP. ABA signalling manipulation suppresses senescence of a leafy vegetable stored at room temperature. Plant Biotechnol J. 2018;16:530–44. https://doi.org/10.1111/pbi.12793.

Reis H, Pfiffi S, Hahn M. Molecular and functional characterization of a secreted lipase from *Botrytis cinerea*. Mol Plant Pathol. 2005;6:257–67. https://doi.org/10.1111/j.1364-3703.2005.00280.x.

Rolke Y, Liu S, Quidde T, Williamson B, Schouten A, Weltring KM, et al. Functional analysis of $H_2O_2$-generating systems in *Botrytis cinerea*: the major Cu-Zn-superoxide dismutase (BCSOD1) contributes to virulence on French bean, whereas a glucose oxidase (BCGOD1) is dispensable. Mol Plant Pathol. 2004;5:17–27. https://doi.org/10.1111/j.1364-3703.2004.00201.x.

Saeed AI, Bhagabati NK, Braisted JC, Liang W, Sharov V, Howe EA, et al. TM4 microarray software suite. Methods Enzymol. 2006;411:134–93. https://doi.org/10.1016/s0076-6879(06)11009-5.

Sandalio LM, Rodríguez-Serrano M, Romero-Puertas MC, del Río LA. Role of peroxisomes as a source of reactive oxygen species (ROS) signaling molecules. In: del Río LA, editor. Peroxisomes and their key role in cellular signaling and metabolism. Netherlands, Dordrecht: Springer; 2013. p. 231–55. https://doi.org/10.1007/978-94-007-6889-5_13.

Schumacher J. Tools for *Botrytis cinerea*: new expression vectors make the gray mold fungus more accessible to cell biology approaches. Fungal Genet Biol. 2012;49:483–97. https://doi.org/10.1016/j.fgb.2012.03.005.

Siegmund U, Viefhues A. Reactive oxygen species in the *Botrytis* - host interaction. In: Fillinger S, Elad Y, editors. *Botrytis* - the fungus, the pathogen and its management in agricultural systems. Cham: Springer International Publishing; 2016. p. 269–89. https://doi.org/10.1007/978-3-319-23371-0_14.

Smith JJ, Aitchison JD. Peroxisomes take shape. Nat Rev Mol Cell Biol. 2013;14:803–17. https://doi.org/10.1038/nrm3700.

Soltis NE, Atwell S, Shi G, Fordyce R, Gwinner R, Gao D, et al. Interactions of tomato and *Botrytis cinerea* genetic diversity: parsing the contributions of host differentiation, domestication, and pathogen variation. Plant Cell. 2019;31:502–19. https://doi.org/10.1105/tpc.18.00857.

Stanley WA, Fodor K, Marti-Renom MA, Schliebs W, Wilmanns M. Protein translocation into peroxisomes by ring-shaped import receptors. FEBS Lett. 2007;581:4795–802. https://doi.org/10.1016/j.febslet.2007.09.001.

Thines E, Weber RW, Talbot NJ. MAP kinase and protein kinase A-dependent mobilization of triacylglycerol and glycogen during appressorium turgor generation by *Magnaporthe grisea*. Plant Cell. 2000;12:1703–18. https://doi.org/10.1105/tpc.12.9.1703.

Tripathi DN, Zhang J, Jing J, Dere R, Walker CL. A new role for ATM in selective autophagy of peroxisomes (pexophagy). Autophagy. 2016;12:711–2. https://doi.org/10.1080/15548627.2015.1123375.

Urban M, Cuzick A, Seager J, Wood V, Rutherford K, Venkatesh SY, et al. PHI-base: the pathogen-host interactions database. Nucleic Acids Res. 2020;48:D613–20. https://doi.org/10.1093/nar/gkz904.

van der Klei IJ, Veenhuis M. The versatility of peroxisome function in filamentous fungi. In: del Río LA, editor. Peroxisomes and their key role in cellular signaling and metabolism. Netherlands, Dordrecht: Springer; 2013. p. 135–52. https://doi.org/10.1007/978-94-007-6889-5_8.

Wanders RJA. Peroxisomes in human health and disease: metabolic pathways, metabolite transport, interplay with other organelles and signal transduction. In: del Río LA, editor. Peroxisomes and their key role in cellular signaling and metabolism. Netherlands, Dordrecht: Springer; 2013. p. 23–44. https://doi.org/10.1007/978-94-007-6889-5_2.

Wang L, Zhang L, Liu C, Sun S, Liu A, Liang Y, et al. The roles of FgPEX2 and FgPEX12 in virulence and lipid metabolism in *Fusarium graminearum*. Fungal Genet Biol. 2020;135: 103288. https://doi.org/10.1016/j.fgb.2019.103288.

Wang ZY, Soanes DM, Kershaw MJ, Talbot NJ. Functional analysis of lipid metabolism in *Magnaporthe grisea* reveals a requirement for peroxisomal fatty acid beta-oxidation during appressorium-mediated plant infection.

Mol Plant Microbe Interact. 2007;20:475–91. https://doi.org/10.1094/mpmi-20-5-0475.
Xu Y, Wang L, Liang W, Liu M. Biocontrol potential of endophytic *Bacillus velezensis* strain QSE-21 against postharvest grey mould of fruit. Biol Control. 2021;161:104711. https://doi.org/10.1016/j.biocontrol.2021.104711.
Zhang L, Wang L, Liang Y, Yu J. FgPEX4 is involved in development, pathogenicity, and cell wall integrity in *Fusarium graminearum*. Curr Genet. 2019;65:747–58. https://doi.org/10.1007/s00294-018-0925-6.